RESEARCH ARTICLE

DOI: 10.54926/jnamt.2025.2524

J Nav Architect Mar Technol 2025;227(1):74-93

Numerical Investigation into the Effects of Initial Stability on the Flooding Dynamics in a Damaged Ro-Pax Ship Model

Mehmet Zeki Şener[1], Hyeon Kyu Yoon[2], Ercan Köse[1], Thi Thanh Diep Nguyen[3], Aeri Cho[4]

[1]Karadeniz Technical University, Department of Naval Architecture and Marine Engineering, Trabzon, Türkiye
[2]Changwon National University, Department of Naval Architecture and Ocean Engineering, Gyeongsangnam-do, South Korea
[3]Changwon National University, Industrial Technology Research Center, Gyeongsangnam-do, South Korea
[4]Changwon National University, Smart Ocean Mobility Engineering, Gyeongsangnam-do, South Korea

To cite this article: M. Z. Şener, H. K. Yoon, E. Köse, T. T. D. Nguyen, and A. Cho. Numerical investigation into the effects of initial stability on the flooding dynamics in a damaged Ro-Pax ship model. *J Nav Architect Mar Technol*. 2025;227(1):74-93.

Received: 03.08.2025 - **Revision Requested:** 10.10.2025 - **Last Revision Received:** 14.10.2025 - **Accepted:** 17.11.2025 - **Publication Date:** 26.12.2025

Abstract

Structural damage to the hull that causes internal flooding poses a significant risk to ship stability, potentially compromising operational integrity and, in severe cases, resulting in capsizing, grounding, or sinking. When water enters through breached compartments, it reduces overall buoyancy and introduces a free-surface effect. Progressive flooding may also occur as water spreads into adjacent compartments through structural openings or failed watertight barriers. The movement of floodwater, combined with fluid–structure interactions, generates complex, nonlinear forces that are difficult to predict. This study employs numerical simulations using a damaged Ro-Pax ship model to examine how initial stability influences flooding behavior and motion response. The analyses are carried out until flooding reaches a quasi-steady state. A Computational Fluid Dynamics methodology is used to accurately capture the fluid–structure interactions during flooding. Two flooding scenarios were simulated with identical damage extents and environmental conditions, but different metacentric height (*GM*) values, to isolate the effect of initial stability. The model's time-dependent linear and angular motions, along with floodwater levels, were monitored throughout the flooding period. Although the affected tanks were not fully filled, the ship model still reached a quasi-steady state. Results indicated that initial *GM* had minimal impact on the total volume of ingress water during the simulation period. This suggests that, given the specific damage geometry and boundary conditions, hydrostatic and hydrodynamic forces primarily govern water ingress, reducing the influence of initial stability. However, notable differences were observed in the motion response. The configuration with lower *GM* exhibited significantly larger roll and yaw motions and lower damping rates. While these dynamic behaviors may not directly affect the volume of floodwater, they have important operational implications, including a higher risk of cargo shift, increased passenger discomfort, and reduced controllability.

Keywords: Damaged stability, flooded ship, Ro-Pax ship, ship dynamics, ship stability

Address for Correspondence: Asst. Prof. Mehmet Zeki Şener, Karadeniz Technical University, Department of Naval Architecture and Marine Engineering, Trabzon, Türkiye
E-mail: senermehmetzeki@ktu.edu.tr
ORCID ID: orcid.org/000-0002-9794-4811

**An earlier version of this paper appeared in the Proceedings of the 3rd International Congress on Ship and Marine Technology (GMO-SHIPMAR 2024, oper source https://www.gmoshipmar.org), 10-12.12.2024, Trabzon, pp. 247–259. The present article is an extended and revised version in which the text and methodology have been refined, and the results are presented in greater detail.*

1. Introduction

Maritime transport is widely used for the carriage of goods and passengers over long distances. The continuous growth in the size and structural complexity of modern ships has increased the importance of damage stability assessments. Among various types of ship damage, flooding is addressed in regulatory frameworks, as it directly influences stability and survivability. Flooding occurs when water enters internal spaces due to structural failure or hull breach. This reduces overall buoyancy and introduces a free-surface effect, both of which affect stability. If not adequately controlled, flooding can result in capsizing, grounding, or total loss of the vessel. To limit the consequences of such events, ships are designed with watertight subdivision and optimized weight distribution to preserve residual stability.

Accurate evaluation of damaged ship stability requires understanding the dynamic interaction between floodwater and ship motion. Progressive flooding through multiple compartments, the location and size of damage openings, the ingress rate of seawater, and the presence of non-watertight internal boundaries all influence the flooding process. Additionally, environmental conditions also introduce dynamic forces that complicate the assessment. These factors necessitate modelling capable of capturing fluid–structure interaction under transient and nonlinear conditions.

Three main approaches are commonly used to evaluate damage stability: experimental, theoretical, and numerical. Each has specific advantages and limitations. Among them, numerical methods offer flexibility in simulating complex geometries and damage scenarios. Computational Fluid Dynamics (CFD), in particular, enables detailed modelling of the fluid behavior and its interaction with ship motion during flooding. CFD has been increasingly applied in maritime research due to improvements in computational capacity. While its predictive capability has been demonstrated in various contexts, further validation is ongoing to ensure its applicability in real-case damage scenarios and regulatory frameworks. The study by Cheng et al. [1] investigated the coupled dynamics between flooding water and damaged ship motion using experimental methods and Smoothed Particle Hydrodynamics (SPH). A refined SPH framework incorporating improved boundary treatments and visualization techniques is developed and validated against physical experiments. The effects of variables such as opening size, position, the number of flooded cabins, and wave conditions were investigated in relation to fluid behavior and ship responses. Results revealed that complex flow structures, including inflow jets, sloshing, and vortex shedding, significantly affect ship stability and motion. Cao et al. [2] developed a SPH model based on strip theory to simulate the dynamic response of a damaged ship in beam seas, accounting for nonlinear interactions between external waves, internal sloshing, and flooding water. The study validated the model using experimental data and conducted parametric analyses on factors such as damage opening size, wave direction, and internal liquid loading. Results showed that flooding-induced damping effects reduced roll motion, and that wave direction relative to the damage opening critically influenced the severity of ship response. Notably, the presence of internal liquid cargo was found to substantially alter sloshing behavior, with a 50% filling ratio minimizing rolling amplitude. Hu et al. [3] conducted a numerical investigation employing a CFD approach that integrates the Navier-Stokes equations with the Volume of Fluid (VOF) method and a dynamic mesh strategy. The simulations were applied to a damaged barge and a rectangular cabin, and the computed results were verified against experimental measurements. The study demonstrated that the applied method effectively captured fluid-structure interaction and flooding dynamics within a time-domain framework. Although not exhaustive, these studies show that as modelling techniques advance, the need for simplifying assumptions decreases.

The complexity of ship flooding increases reliance on CFD-based simulations. However, recent advancements in CFD techniques have broadened their range of applications. To implement CFD effectively in these scenarios, a thorough understanding of the available numerical methods is essential. Wang and Wan [4] reviewed the advancements in CFD for predicting complex viscous flows around floating structures, highlighting techniques such as the VOF method, dynamic overset grid, and fluid-structure coupling. Similarly, Xu et al. [5] discussed numerical simulation techniques for various hydrodynamic coupling problems, including hull-propeller-rudder coupling, wave-floating structure coupling, aerodynamic-hydrodynamic coupling, fluid-structure coupling, and fluid-noise coupling. The paper emphasizes the importance of accurately predicting these coupling effects to optimize ship and ocean engineering designs. In this context, Çakıcı et al. [6] utilized the URANS method to compute hydrodynamic coefficients for heave motion of a Wigley hull with forward speed, demonstrating that viscous flow solutions offer higher accuracy than potential flow methods, particularly regarding damping characteristics. These studies underscore the advancements in CFD methods for resolving complex fluid-structure interactions and improving computational efficiency.

1.1. Aim of the Study

Structural breaches in the hull can lead to flooding, which may subsequently spread through internal openings and failed doors and hatches. The spread of floodwater decreases buoyancy and induces a free-surface effect, both of which significantly impair stability. Assessing the stability of

a damaged ship is inherently complex due to the coupled dynamics between internal flooding and ship motion. The resulting fluid–structure interactions generate nonlinear forces that are difficult to model using conventional assessment methods.

The International Maritime Organization (IMO) provides a regulatory framework for damage stability assessment by prescribing standardized damage scenarios and probabilistic calculation methods. These approaches typically assume instantaneous flooding and do not incorporate the time-dependent progression of water ingress or the associated motion responses of the ship. As a result, such methods may not adequately represent the physical realities of damaged ship behavior, particularly in dynamic sea states or during complex flooding events.

This study aims to address these limitations by applying numerical simulations based on CFD to evaluate the dynamic behavior of a Ro-Pax ship model under two distinct initial metacentric height (*GM*) conditions. The simulations are conducted under identical external and internal damage parameters, enabling a controlled comparison of vessel responses. The objective is to provide a detailed representation of stability under damaged conditions, thereby supporting the potential use of CFD in early-stage ship design and contributing to the refinement of performance-based stability assessment methods.

2. Materials and Methods

Stability analysis of damaged ships under flooding conditions requires accurate modeling of fluid–structure interaction and motion response. Depending on the objectives and constraints of a given study, different methodological frameworks may be employed. In this study, internal flooding and resulting ship motions are simulated using a Unsteady Reynolds-Averaged Navier-Stokes-URANS-based CFD approach. This section provides a detailed explanation of the materials and methods used in this study, along with their application procedures.

2.1. Damage Stability of Ships

Damage stability is the capacity of a vessel to remain afloat and maintain equilibrium after sustaining structural damage that allows water to ingress into one or more watertight compartments while complying with regulatory standards set by International Convention for the Safety of Life at Sea-SOLAS and IMO guidelines. When the watertight hull is breached, floodwater increases the weight of the vessel and reduces the buoyant volume. This can significantly compromise stability and pose serious risks to the ship, the passengers, the crew, and the cargo. Under severe flooding conditions, uncontrolled flooding leads to insufficient buoyancy and a high probability of capsizing or sinking.

Major maritime disasters acted as pivotal moments that shaped the development of modern damage stability regulations. High-profile incidents revealed the catastrophic consequences of inadequate subdivision and insufficient flood survivability, prompting a global shift in regulatory priorities. As a result, international safety frameworks such as SOLAS Chapter II-1 and guidelines set forth by the IMO require ships to be designed with sufficient watertight subdivision and residual stability. The goal is to ensure that vessels can remain afloat and upright even after sustaining damage. These regulations are not only essential for passenger ships but also apply to cargo vessels, tankers, and specialized offshore units. Through both deterministic and probabilistic approaches, naval architects must demonstrate that a vessel can survive specific damage conditions without exceeding allowable heel angles or stability thresholds, thereby safeguarding human life, cargo, and the marine environment.

Understanding stability in normal conditions is essential for evaluating how a vessel reacts to damage. Stability refers to the ability of a ship to resist heeling caused by external forces and to return to an upright position once those forces are removed. This behavior depends on the relationship between the center of gravity, the center of buoyancy, and the metacenter. When a vessel is upright, the center of gravity and the center of buoyancy are vertically aligned. As the vessel heels, the center of buoyancy shifts laterally due to the change in the shape and distribution of the submerged volume. The intersection between the vertical line of buoyant force and the initial centerline defines the metacenter.

GM, defined as the distance between the center of gravity and the metacenter, is a parameter for evaluating initial ship stability. Greater *GM* typically results in stronger resistance to heeling and faster righting action in response to disturbances. Beyond static considerations, *GM* also plays a role in the vessel response during compartment flooding. When a vessel experiences asymmetrical flooding, internal water movement creates free-surface moments that reduce effective transverse stability. This reduction in *GM* leads to greater roll angles and can increase the risk of capsizing. While the amount of water entering damaged compartments is mainly governed by factors such as breach geometry and hydrostatic pressure, *GM* significantly affects the motion response of the vessel. Characteristics such as roll amplitude, period, and damping behavior are strongly influenced by *GM*, especially during transient flooding conditions. Reduced *GM* are more susceptible to rapid capsize following flooding incidents. In such cases, safety margins decrease, and the time available for evacuation is often insufficient. Therefore, assessing *GM* within both static and dynamic frameworks is essential for comprehensive damage stability analysis.

CFD simulations are important for advancing ship design and safety evaluation. They enable the creation of a virtual yet realistic environment for the effective testing of various conditions. In this study, CFD simulations were used to assess the impact of two different initial stability conditions on a Ro-Pax vessel model. The primary aim was to examine how these conditions influence the progression of flooding and, in turn, affect the motion response. Since initial stability plays a major role in ship dynamics, analyzing this parameter is essential for enhancing overall ship safety.

2.2. Numerical Methodology

Fluid dynamics investigates the motion of substances such as liquids and gases, which do not resist deformation when subjected to external shear forces. To analyze fluid flow, the control volume approach provides a practical and convenient framework. By focusing on a defined control volume, fundamental conservation laws, such as mass, momentum, and energy, can be systematically derived.

The Navier-Stokes equations, named after Claude-Louis Navier [7] and George Gabriel Stokes [8], offer a comprehensive description of the motion of viscous fluids. These equations define how velocity, pressure, temperature, and density interact in a moving fluid. The conservation of momentum expressed in the Navier-Stokes equations corresponds to Newton's second law applied to a fluid element, incorporating forces due to pressure, viscosity, and external influences such as gravity. Although these nonlinear partial differential equations are widely applied in science and engineering, they remain one of the most challenging aspects of fluid dynamics due to their mathematical complexity.

The Navier-Stokes equations for an incompressible three-dimensional flow can be written as follows (Equation 1):

$$\frac{\partial \vec{U}}{\partial t} + (\vec{U} \cdot \nabla)\vec{U} = g - \frac{1}{\rho}\nabla P + \nu \nabla^2 \vec{U} \quad (1)$$

where "∇^2" is the Laplacian or Laplace operator.

Applying the Navier-Stokes equations in practical scenarios often requires the use of numerical methods due to the inherent complexity of obtaining analytical solutions. CFD techniques enable the approximation of solutions to the Navier-Stokes equations across a wide range of flow regimes and geometries. Despite their effectiveness, these methods reveal the inherent complexity of the equations, and finding exact solutions remains a major challenge. This difficulty is embodied in one of the most renowned unsolved problems in mathematics: the Navier-Stokes existence and smoothness problem.

The Navier–Stokes equations form the basis for describing fluid motion. However, due to the mathematical complexity of these equations, simplifications are often required to enable practical implementation in engineering applications. This need for simplification leads to the use of the Reynolds-Averaged Navier-Stokes (RANS) equations. Named after Osborne Reynolds [9], these equations provide a framework for addressing the challenges of turbulent flow analysis. By averaging flow properties over time, RANS equations reduce the complexity of the system while still capturing the essential effects of turbulence. This approach enables the prediction of the average behaviour of turbulent flows.

The RANS equations are derived from the original Navier-Stokes equations using Reynolds decomposition, which separates flow variables into a time-averaged component and a fluctuating component. This methodology removes instantaneous turbulent fluctuations and replaces them with their averaged effect, thereby simplifying the equations. The momentum equation for incompressible flow can be expressed as follows (Equation 2):

$$\frac{\partial}{\partial t}(\rho \overline{u}_i) + \frac{\partial}{\partial x_j}(\rho \overline{u}_i \overline{u}_j) = -\frac{\partial P}{\partial x_i} + \frac{\partial}{\partial x_i}[\mu(\frac{\partial \overline{u}_i}{\partial x_j} + \frac{\partial \overline{u}_j}{\partial x_i} - \frac{2}{3}\delta_{ij}\frac{\partial \overline{u}_i}{\partial x_i})] + \frac{\partial}{\partial x_j}(-\rho \overline{u_i'}\,\overline{u_j'}) \quad (2)$$

In these equations, $\overline{u}_i$ and $\overline{u}_j$ represent the mean average flow velocities, $\overline{u_i'}$ and $\overline{u_j'}$ denote the fluctuating velocities, μ is the dynamic viscosity, ρ is the fluid density, δ_{ij} is the Kronecker delta function, and P is fluid pressure.

The conservation of mass refers to the principle that the total mass within a system remains constant over time. This fundamental concept forms the basis for understanding and analysing fluid flow in a wide range of engineering and physical applications. It is commonly expressed through the continuity equation, which states that the mass entering a control volume must equal the mass exiting it, assuming there is no accumulation or loss of mass within the volume.

For Newtonian fluids, the mass continuity equation can be expressed as follows (Equations 3-5):

$$\dot{m} = \frac{\partial m}{\partial t} = \int_v \frac{\partial \rho}{\partial t} dv = 0 \quad (3)$$

$$\int_v \left[\frac{\partial \rho}{\partial t} + \nabla \cdot \left(\rho \vec{U}\right)\right] = 0 \quad (4)$$

$$\frac{\partial \rho}{\partial t} + \nabla \cdot \left(\rho \vec{U}\right) = 0 \quad (5)$$

where ρ is the density, $\vec{U}$ is the vector for flow velocity in three-dimensional cartesian coordinates. ∇ represents the divergence operator, and Equation (5) can be expanded as (Equation 6):

$$\frac{\partial \rho}{\partial t} + \frac{\partial (\rho u)}{\partial x} + \frac{\partial (\rho v)}{\partial y} + \frac{\partial (\rho w)}{\partial z} = 0 \quad (6)$$

In fluid dynamics, certain scenarios permit the assumption of constant fluid density, giving rise to the concept of

incompressible flow. This assumption greatly simplifies the governing equations and serves as the foundation for many practical applications. Incompressibility is commonly associated with liquids, which exhibit very low compressibility. Although the incompressible flow model is widely used, it should only be applied when compressibility effects are negligible. In this study, the incompressible flow model is employed for understanding the process of compartment flooding in damaged ships. By reducing the complexity of the governing equations, the incompressible flow model offers a more practical approach.

A fluid is considered incompressible when its density remains constant, as expressed by the following condition (Equation 7):

$$\frac{\partial(\rho u)}{\partial x} + \frac{\partial(\rho v)}{\partial y} + \frac{\partial(\rho w)}{\partial z} = 0 \quad (7)$$

Turbulence closure models account for the Reynolds stresses by modelling the transfer of energy between the mean and turbulent flows, addressing the closure problem in the Reynolds-averaged equations. To achieve closure, higher-order terms must be expressed in terms of lower-order quantities, ensuring the number of equations matches the number of unknowns.

Boussinesq [10] proposed that turbulence fluctuations could be modelled using the concept of eddy viscosity, a flow property rather than a physical property of the fluid. Prandtl [11] extended this idea by introducing the notion that eddy viscosity is not constant but varies depending on the local rate of strain and turbulence scale. This development led to the formulation of turbulence models, where additional transport equations are solved to determine local turbulence characteristics. One-equation turbulence models solve a single transport equation for turbulent kinetic energy (k), offering reasonable accuracy for many turbulent flows while maintaining computational efficiency. In comparison, two-equation models solve two transport equations, typically for turbulent kinetic energy and a second variable related to the turbulence length scale.

In this study, ANSYS Fluent was used to simulate the flooding process by combining the VOF model with the overset grid technique and a six-degree-of-freedom solver. The VOF model enables the simulation of two or more immiscible fluids by tracking the volume fraction of each. The overset grid method offers flexibility in handling complex geometries and moving boundaries without requiring frequent remeshing. This combination facilitated the simulation of fluid-structure interactions during compartment flooding and captured the ship's motion response. The continuity and momentum equations, along with the k-omega Shear Stress Transport (SST) turbulence model, were employed to analyse fluid flow, while the VOF model determined the volume fractions of air and water. This methodology provided an accurate representation of the turbulent, multiphase flow dynamics involved in the flooding scenario.

The k-ω SST model defines both turbulent kinetic energy (k) and the specific dissipation rate (ω). The modelled transport equations for the k-ω SST formulation are as follows (Equations 8 and 9) [12]:

$$\frac{\partial}{\partial t}(\rho k) + \frac{\partial}{\partial x_i}(\rho k \overline{u_i}) = \frac{\partial}{\partial x_j}\left[\left(\mu + \frac{\mu_t}{\sigma_k}\right)\frac{\partial k}{\partial x_j}\right] + G_k - Y_k + S_k \quad (8)$$

$$\frac{\partial}{\partial t}(\rho \omega) + \frac{\partial}{\partial x_i}(\rho \omega \overline{u_i}) = \frac{\partial}{\partial x_j}\left[\left(\frac{\mu + \mu_t}{\sigma_\omega}\right)\frac{\partial \omega}{\partial x_j}\right] + G_\omega - Y_\omega + D_\omega + S_\omega \quad (9)$$

In these equations, G_k represents the generation of turbulence kinetic energy due to average velocity gradients, while G_ω denotes the production of ω. The terms Y_k and Y_ω account for the dissipation of k and ω due to turbulence, respectively. The source terms are represented by S_k and S_ω which representing external influences affecting k and ω. The turbulence Prandtl numbers for k and ω are given by σ_k and σ_ω. Additionally, D_ω is the cross-diffusion term. The turbulent viscosity (μ_t) for the SST k-ω model is given by (Equation 10) [11]:

$$\mu_t = \frac{(\rho k/\omega)}{max\left[\frac{1}{\alpha^*}, \frac{\Omega F_2}{\alpha_1 \omega}\right]} \quad (10)$$

In this equation, Ω represents the strain rate magnitude, and α^* is a coefficient used to dampen turbulent viscosity. The turbulent Prandtl numbers σ_k ve σ_ω for k and ω are used as follows: $\sigma_{k,1} = 1.176$, $\sigma_{\omega,1} = 2.0$, $\sigma_{k,2} = 1.0$, $\sigma_{\omega,2} = 1.168$, $\alpha_1 = 0.31$.

2.3. Geometry and Mesh Structure

Accurate model design is required for reliable structural assessment and flooding analysis. Model must include all dimensions and structural elements that directly affect hydrostatic and hydrodynamic behavior, such as hull shape and compartment boundaries. The numerical model should apply appropriate boundary conditions and capture fluid–structure interaction relevant to flooding scenarios.

Table 1. Main dimensions of the ship model

Main dimensions	
Overall length, L_{OA}	1.435 m
Length between perpendiculars, L_{PP}	1.310 m
Beam, B	0.250 m
Draft, T	0.054 m
GM_1	0.03121 m
GM_2	0.02455 m

GM: Metacentric height

Table 2. Main dimension of the compartments			
Compartments	**Length [m]**	**Width [m]**	**Depth [m]**
Compartment 1	0.119	0.250	0.066
Compartment 2	0.119	0.250	0.066
Compartment 3	0.066	0.250	0.066

This study uses a model of a 162-meter Ro-Pax vessel [13] developed by Meyer Turku Shipyard [14], in accordance with SOLAS safety standards [15]. Ro-Pax vessels are frequently used in flooding studies due to their open vehicle decks, which allow water accumulation and can significantly reduce transverse stability under asymmetric damage. The vessel's main dimensions and compartment configuration are provided in Table 1 and Table 2.

The first step in numerical simulations is the generation of model geometry. At this stage, the physical system is simplified into a form suitable for numerical analysis. The components and features of the system are defined in accordance with the objectives of the study, ensuring that the model accurately represents the essential aspects of the problem while omitting irrelevant details. The model prepared for simulation is illustrated in Figures 1a and 1b.

It is recommended to represent the damage opening using a simple geometric shape, such as a triangle, a rectangle, or a trapezoid [16]. Accordingly, compartments 2 and 3

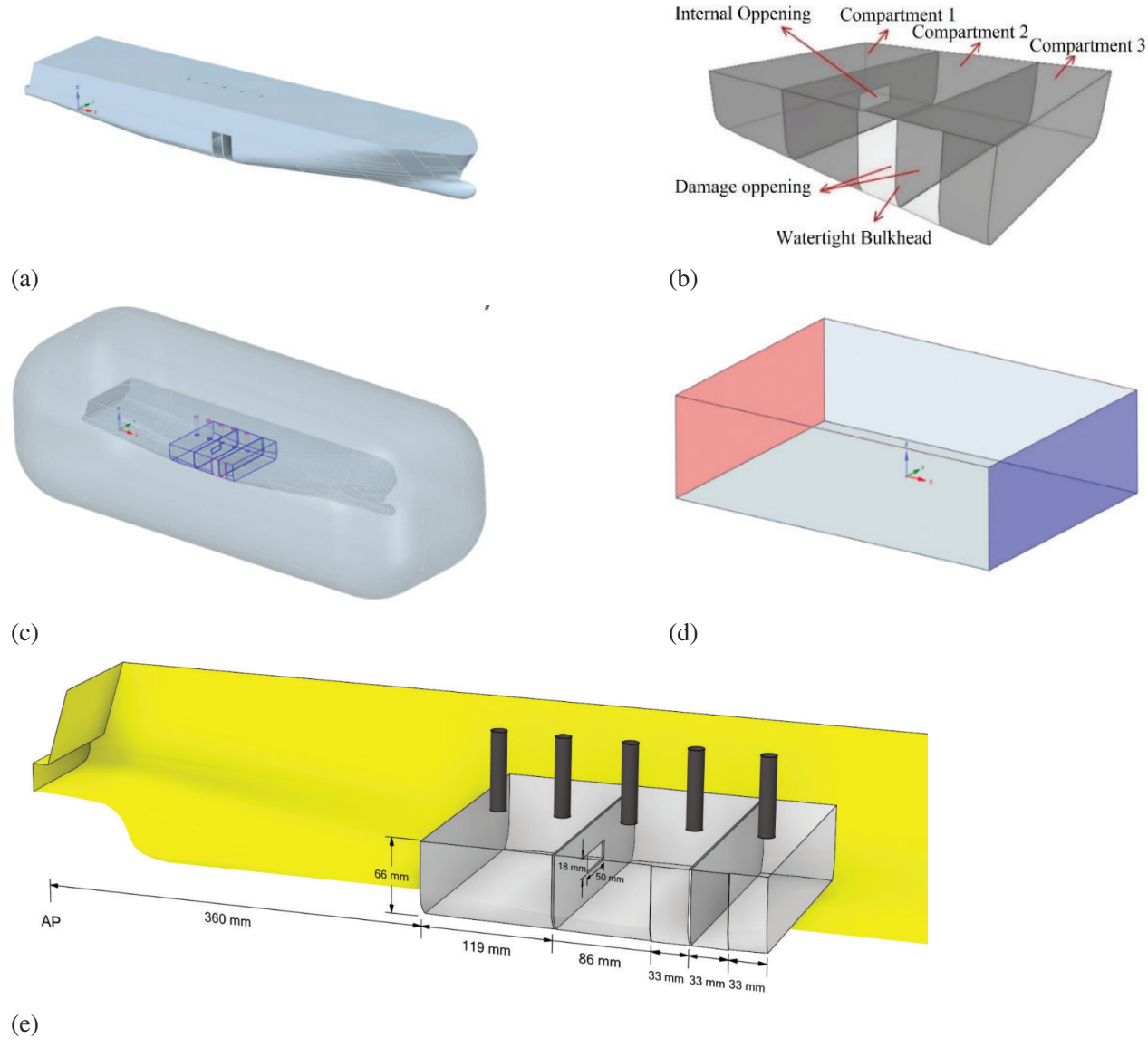

Figure 1. Illustrations of ship structure and zones: **(a)** ship model, **(b)** flooding compartments, **(c)** component zone, **(d)** background zone, and **(e)** compartment layout

in the ship's hull each include a continuous opening with a width of 33 mm to represent the damaged area. The height of the damage extends from the top to the bottom of the compartment, allowing unobstructed water ingress. To ensure proper ventilation and prevent air entrapment, airflow channels with a diameter of 15 mm have been incorporated.

Mesh generation is the process of discretizing the physical domain into smaller, finite cells, enabling the numerical solution of the governing equations over the computational domain. The mesh quality and resolution directly affect both the accuracy of the numerical solution and the computational cost. Higher mesh density is applied in regions with complex flow behavior or strong fluid-structure interactions, such as near the hull surface, inside the damaged compartments, and along the free surface interface. In contrast, lower mesh density is used in areas with relatively uniform flow, such as regions distant from the hull or away from the free surface. This mesh distribution improves accuracy in zones where large velocity or pressure gradients are expected, while limiting the total cell count and maintaining computational efficiency. The mesh structure was configured to balance numerical precision with simulation performance. An overset mesh approach is employed to simulate interactions between components exhibiting relative motion, including translation and rotation. In this method, individual mesh zones are generated for separate parts of the domain, and data is exchanged between them through interpolation. This strategy supports simulations involving time-dependent geometries and enables localized refinement. In the present study, two mesh zones were created, as shown in Figures 1c and 1d. The component mesh consists of 1,671,554 cells, and the background mesh, which covers a domain of 20 m×14 m×1.8 m, comprises 1,476,620 cells, as illustrated in Figure 2.

2.4. Boundary Conditions and Numerical Setup

The definition of boundary conditions involves specifying the physical and environmental constraints applied to the model to reflect the conditions of the actual system. These inputs influence the flow behavior and solution stability within the computational domain and affect the reliability of the simulation results. The selection of boundary conditions is based on the characteristics of the system and the specific objectives of the simulation. This includes the assignment of parameters such as pressure, temperature, velocity, and turbulence properties at relevant boundaries. Once defined,

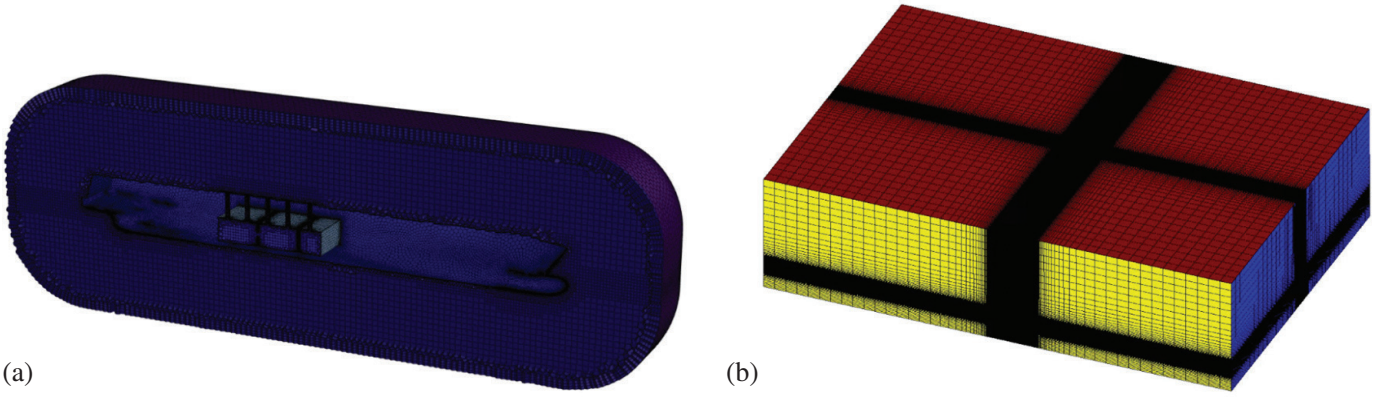

(a) (b)

Figure 2. Meshes for the **(a)** component zone and **(b)** background zone

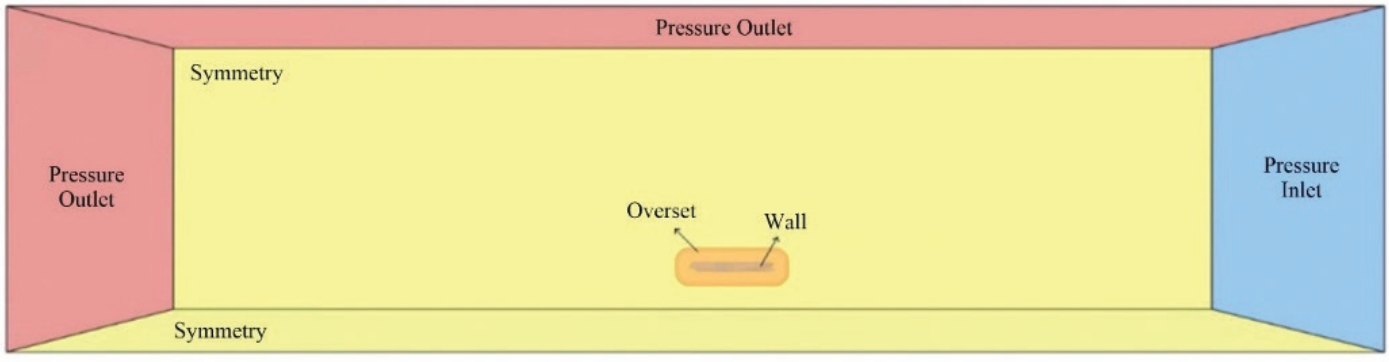

Figure 3. Boundary conditions for the computational domain

the boundary conditions are implemented in the simulation environment. The boundary conditions applied in this study are shown in Figure 3.

The turbulence model employed in the simulations is the k-ω SST model. This model combines the advantages of the standard k-ε and k-ω formulations and is suitable for capturing the behavior of boundary layers under adverse pressure gradients and separating flows. It solves transport equations for the turbulent kinetic energy (k) and the specific dissipation rate (ω), enabling accurate representation of turbulence effects both near the wall and in the free stream. The k-ω SST model is widely used in engineering applications due to its robustness in handling a broad range of Reynolds numbers and its ability to model complex flow features, including wall-bounded flows, flow separation, and recirculation.

Analytical solutions of non-linear partial differential equations are generally not feasible for most practical flow problems. Therefore, CFD relies on numerical methods, such as the finite volume method, to obtain approximate solutions. In this approach, the flow domain is discretized into control volumes, over which the governing equations are integrated to yield algebraic equations defined at the centroids of the volumes. Interpolation schemes are applied to estimate variable values at the control volume faces using the centroid values. In this study, a second-order upwind scheme is used to improve the spatial accuracy of the convective terms. For transient simulations, the solution is advanced in time using a fixed time step of 0.002 s to capture unsteady flow behavior. The coupled algorithm, an iterative pressure-velocity coupling method, is employed to solve the resulting system of equations until convergence is achieved.

3. Results and Discussion

This study examines the influence of initial GM on the flooding behavior and motion response of a damaged Ro-Pax vessel through RANS-based CFD simulations. The objective is to evaluate how variations in initial stability affect the rate of water ingress and the ship's dynamic response during flooding. Two stability configurations, GM_1 and GM_2, are analyzed to compare the temporal evolution of floodwater and the corresponding motion characteristics of the vessel. This section presents the simulation results, including trends in floodwater accumulation and ship motion, and discusses their implications for the damaged stability performance of Ro-Pax ships.

The mass of floodwater increases over time for both GM_1 and GM_2 cases, with no significant deviation observed between the two configurations. This indicates that, within the tested range, variations in initial GM have a negligible effect on the rate of water ingress. As shown in the figure, the floodwater mass stabilizes at approximately 3.6 kg for both cases after around 10 seconds (Figure 4). The close alignment of the two curves suggests that the initial stability condition does not substantially influence the flooding progression within the considered timeframe.

The angular motion responses under the initial stability conditions GM_1 and GM_2 are presented in Figure 5. As shown in Figure 5a, GM_2 exhibits a higher initial roll amplitude compared to GM_1, reflecting the influence of lower GM on roll behavior. Over time, both configurations display roll damping, with decreasing roll amplitudes that converge to near-zero values by approximately 8 seconds. The comparison indicates that higher initial GM_1 results in reduced maximum roll angles during the flooding process. These findings

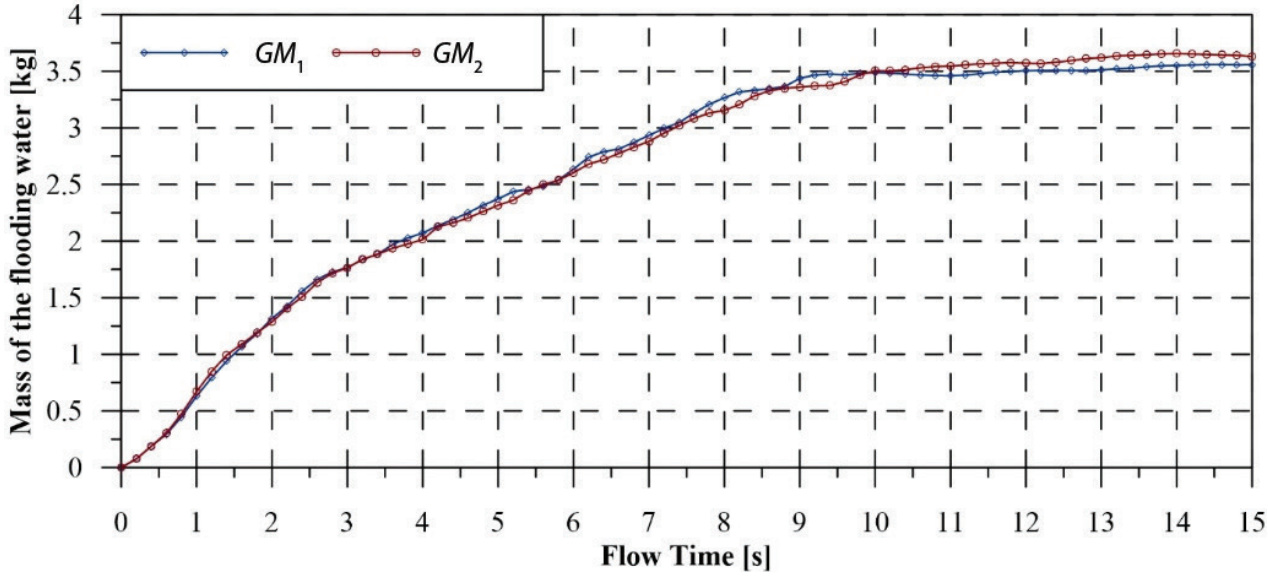

Figure 4. Mass of the flooding water under the initial stability conditions of GM_1 and GM_2

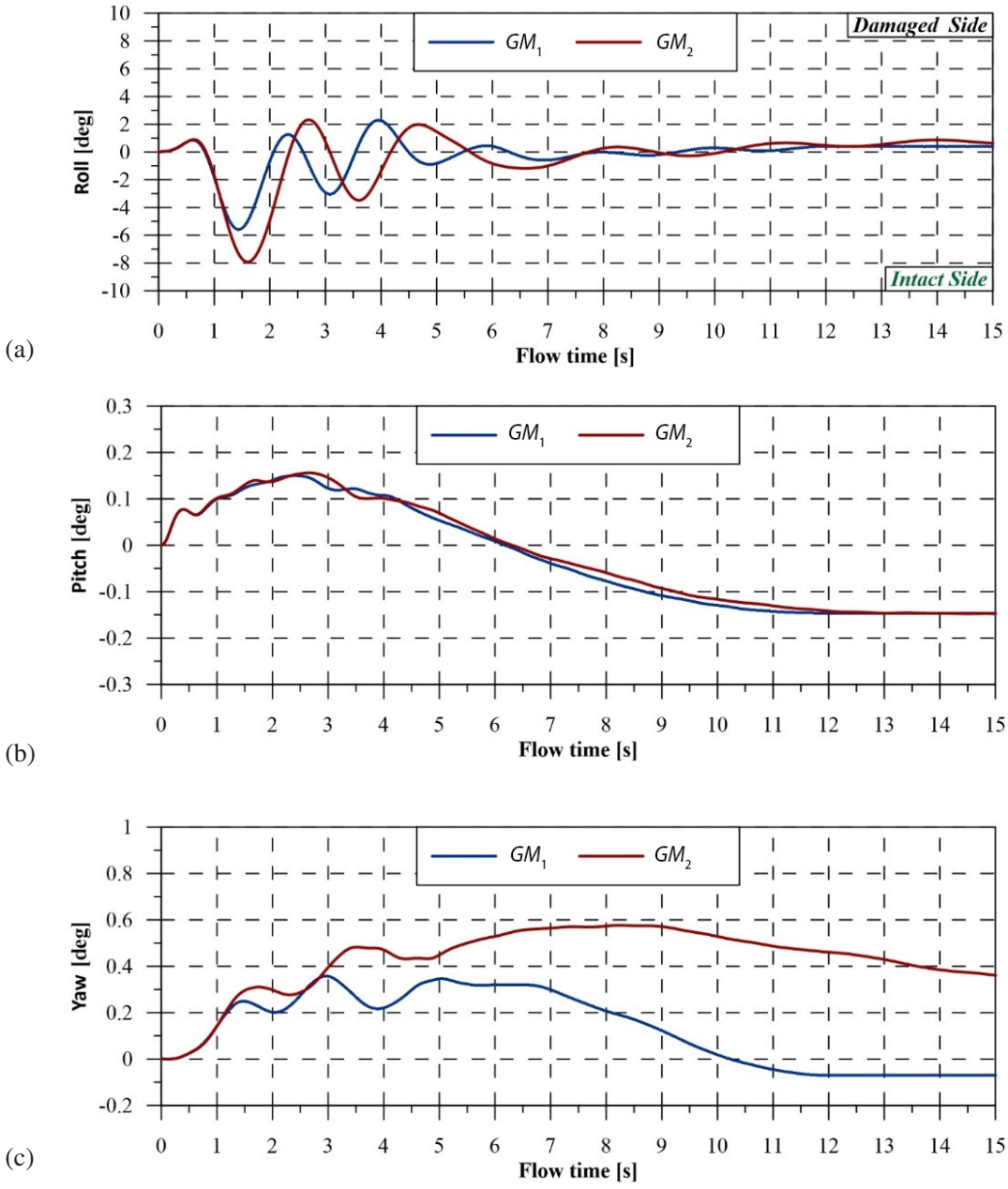

Figure 5. The angular motion responses during flooding under the initial stability conditions of GM_1 and GM_2: **(a)** roll, **(b)** pitch, and **(c)** yaw

highlight the role of initial stability in determining the ship's roll response under damaged conditions. A higher *GM* value contributes to lower roll amplitudes in the early stages of flooding, which may reduce the likelihood of cargo shift, particularly for wheeled cargo commonly transported on Ro-Pax vessels. However, maintaining an optimal *GM* must be considered in the context of overall vessel design and operational constraints, as excessively high stability can lead to reduced comfort and operational flexibility.

The linear motion responses for the initial stability conditions GM_1 and GM_2 are presented in Figure 6. In the surge direction, both configurations exhibit similar behavior throughout the flooding event. During the initial phase (0-3 seconds), surge displacements remain close to zero with minor oscillations. As flooding progresses, the surge response increases in both cases, reaching a peak near 8 seconds. After this point, a gradual reduction is observed, with surge displacement stabilizing around -7 mm by the end of the simulation period. In contrast, the sway motion response reveals more notable differences between the two configurations. While initial displacements are comparable, divergence becomes evident as flooding continues. GM_2,

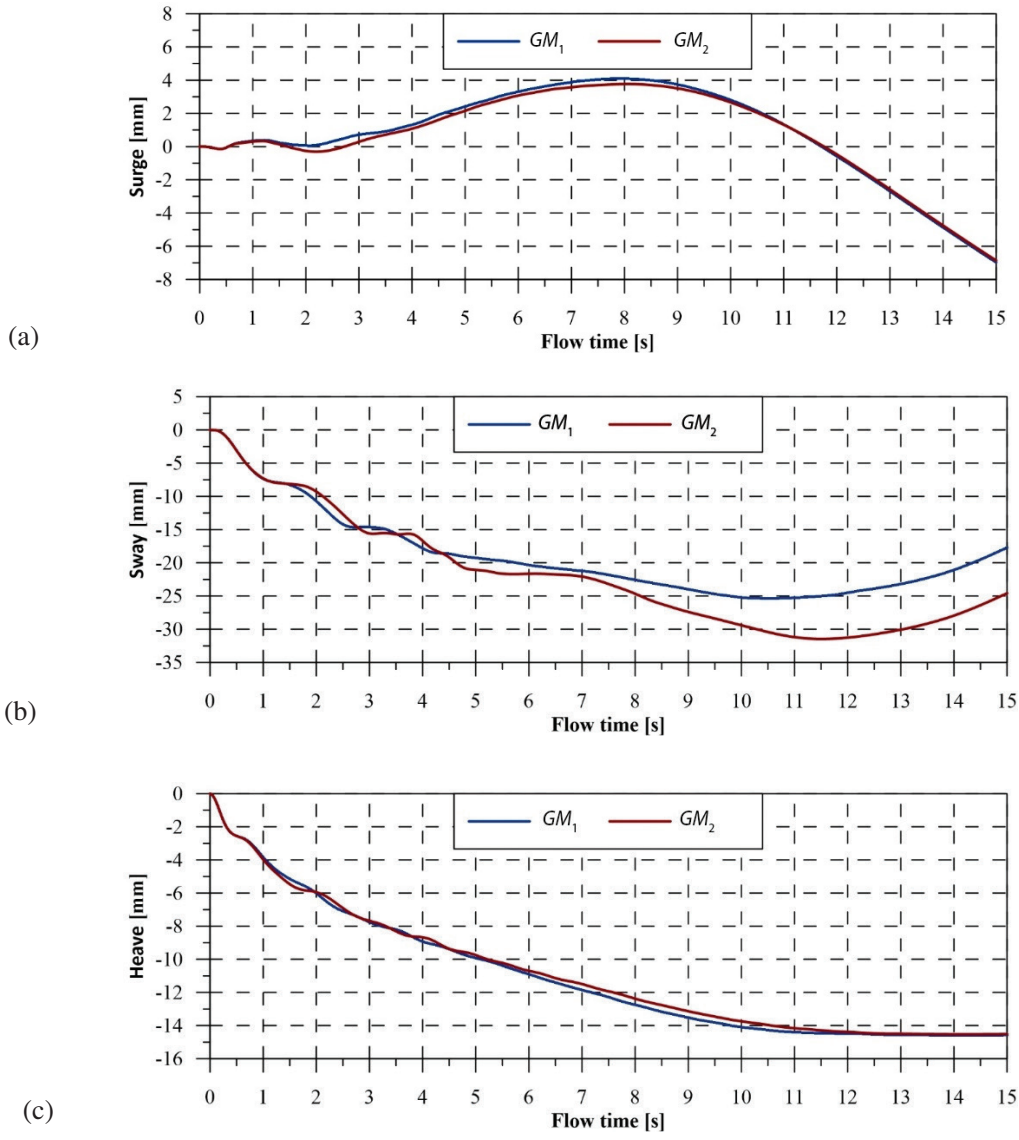

Figure 6. The linear motion responses during flooding under the initial stability conditions of GM_1 and GM_2: **(a)** surge, **(b)** sway, and **(c)** heave

representing the lower initial stability case, reaches a maximum negative sway displacement of over -30 mm at approximately 7 seconds, whereas GM_1 reaches around -25 mm at the same time. This suggests that lower initial *GM* is associated with greater lateral movement during flooding. In the later stages, both configurations exhibit damping behavior, with sway displacements gradually returning toward less negative values.

The heave motion response shows a consistent trend for both GM_1 and GM_2. Initially, both cases experience a gradual downward (negative) displacement, which continues until approximately 10 seconds, reaching around -14 mm. Toward the end of the simulation period, the heave displacement stabilizes at approximately -15 mm for both configurations, indicating convergence and a steady-state condition.

Figure 7 and Figure 8 presents the temporal evolution of the flooding process for the initial stability configurations GM_1 and GM_2. The velocity field of the floodwater (Figure 7) is visualized using a color scale, where blue represents low velocities and red indicates high velocities. At the onset of flooding, water enters the empty compartments through the damaged opening, resulting in a rising water level and increasing flow velocity. As the flooding progresses, the flow becomes more uniformly distributed across Compartments 2 and 3. With continued ingress, water enters Compartment 1, during which the velocity magnitudes begin to decrease. Once Compartment 1 is substantially flooded, the flow field stabilizes. In the final stages, the flooding reaches a quasi-steady state, characterized by relatively uniform water distribution and reduced velocity variations across the compartments.

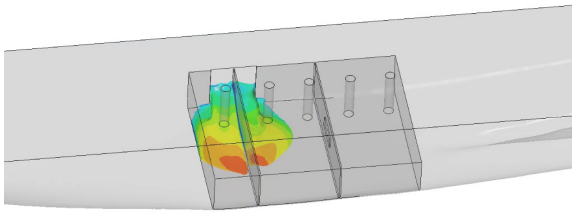

GM_1, t=0.2 s

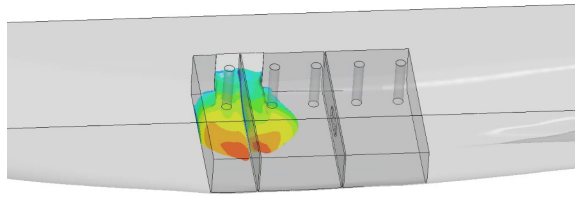

GM_2, t=0.2 s

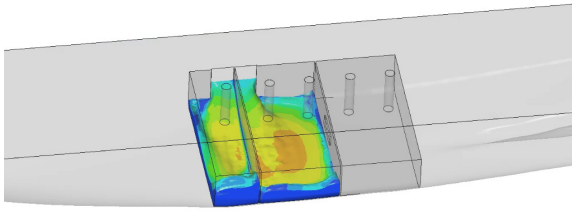

GM_1, t=0.6 s

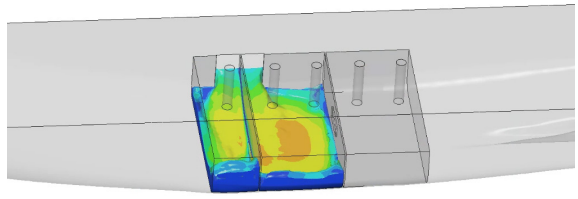

GM_2, t=0.6 s

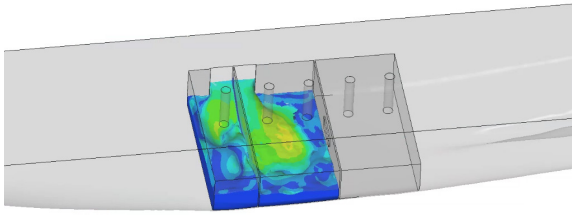

GM_1, t=1.0 s

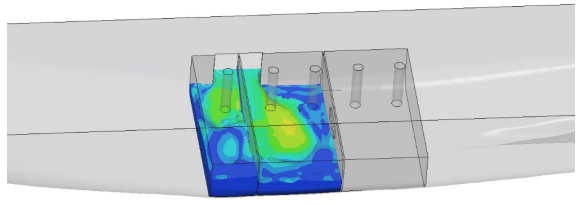

GM_2, t=1.0 s

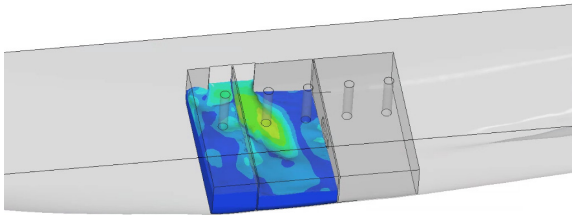

GM_1, t=1.4 s

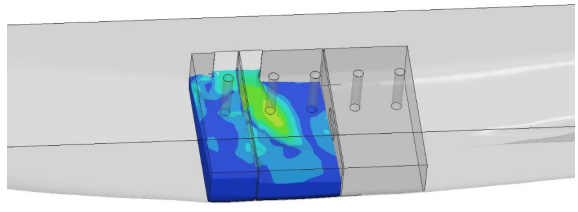

GM_2, t=1.4 s

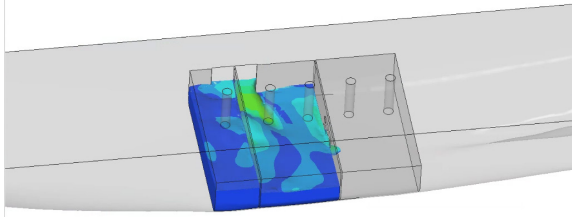

GM_1, t=1.8 s

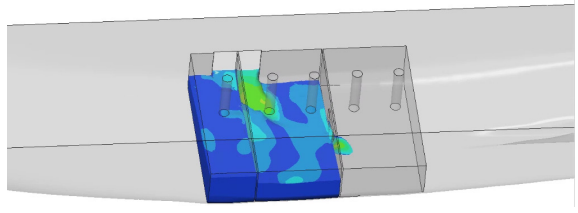

GM_2, t=1.8 s

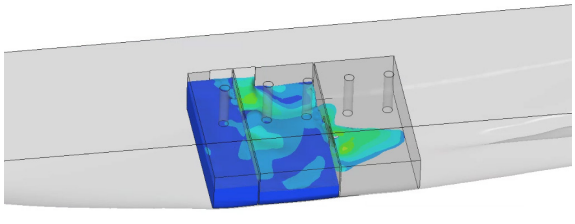

GM_1, t=2.2 s

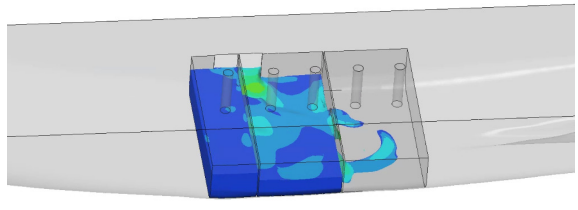

GM_2, t=2.2 s

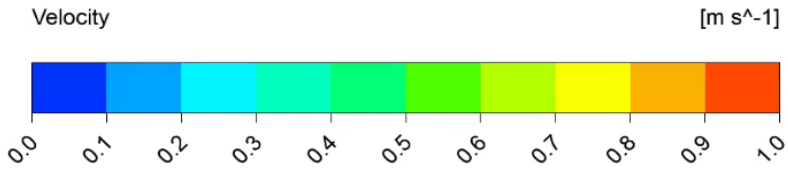

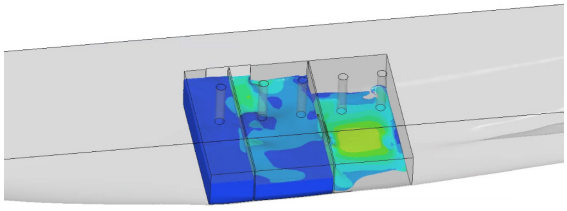

GM_1, t=2.6 s

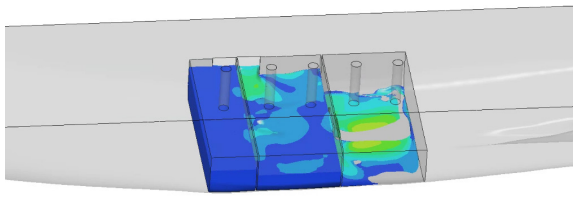

GM_2, t=2.6 s

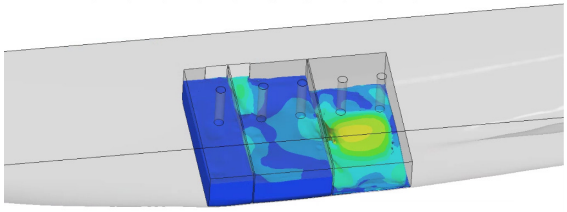

GM_1, t=3.0 s

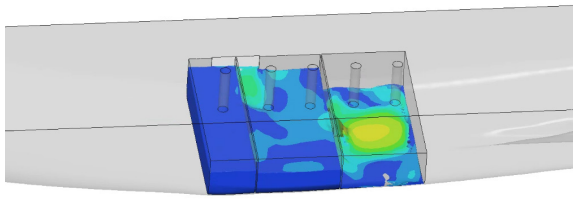

G GM_2, t=3.0 s

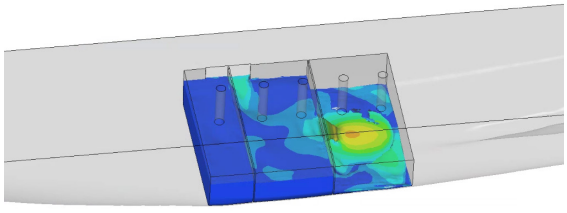

GM_1, t=3.4 s

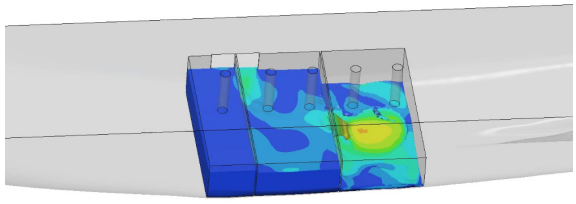

GM_2, t=3.4 s

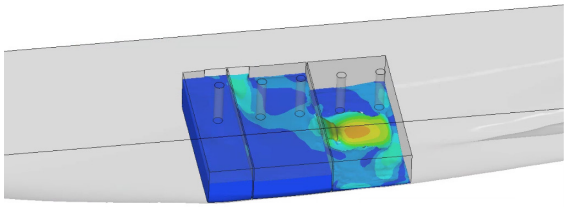

GM_1, t=3.8 s

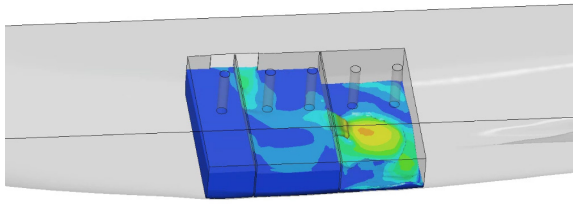

GM_2, t=3.8 s

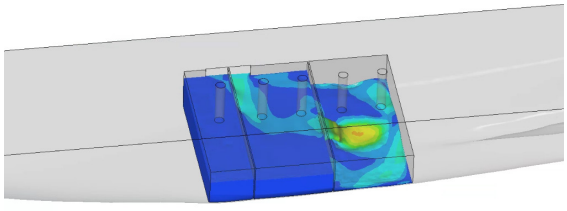

GM_1, t=4.2 s

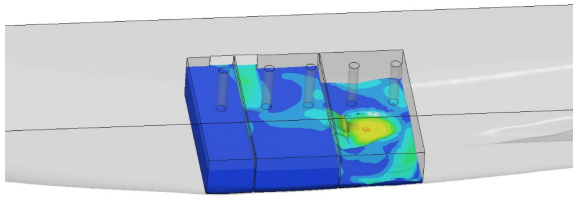

GM_2, t=4.2 s

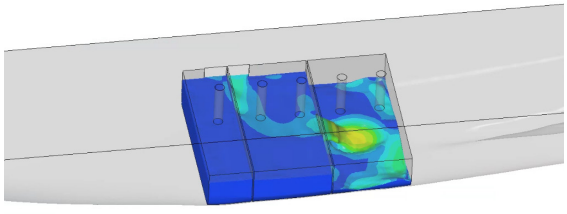

GM_1, t=4.6 s

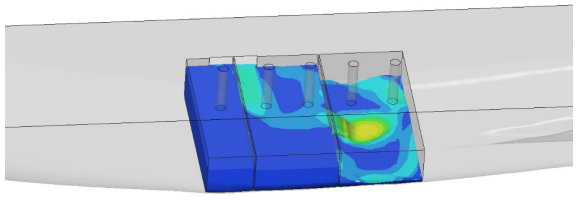

GM_2, t=4.6 s

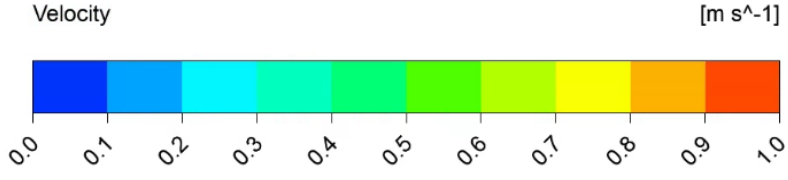

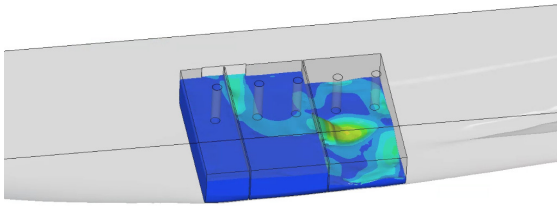

GM_1, t=5.0 s

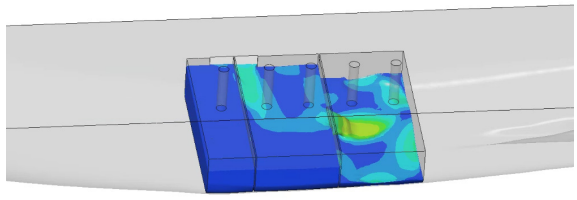

GM_2, t=5.0s

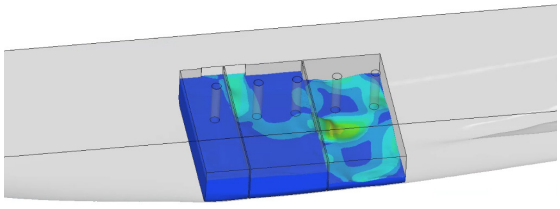

GM_1, t=5.4 s

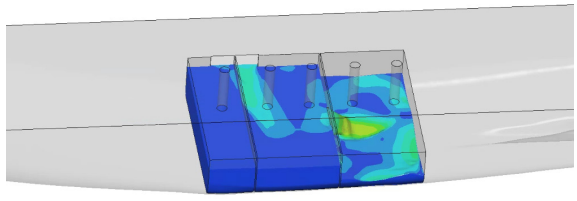

GM_2, t=5.4 s

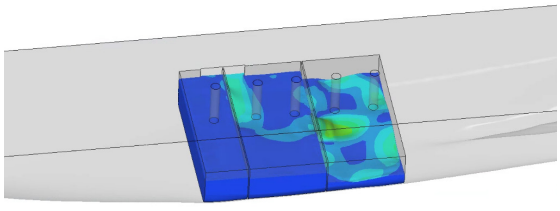

GM_1, t=5.8 s

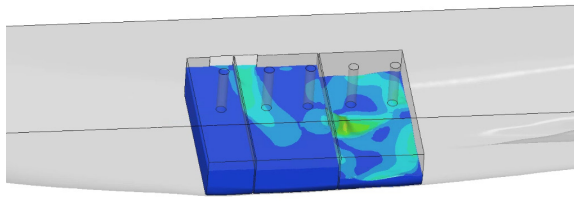

GM_2, t=5.8 s

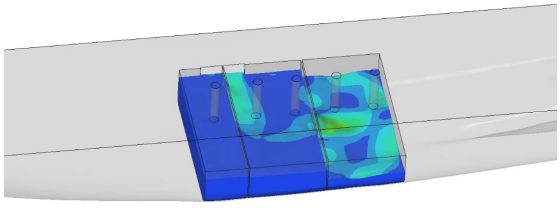

GM_1, t=6.2 s

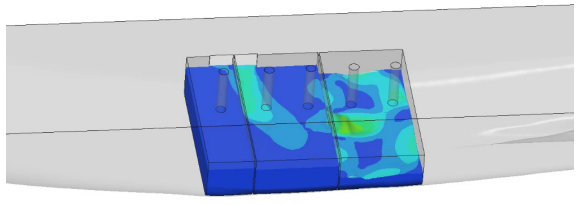

GM_2, t=6.2 s

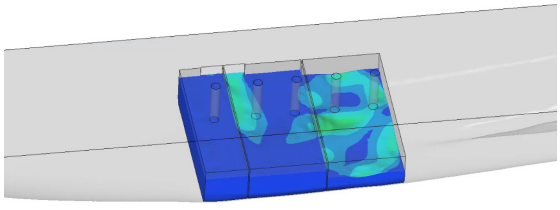

GM_1, t=6.6 s

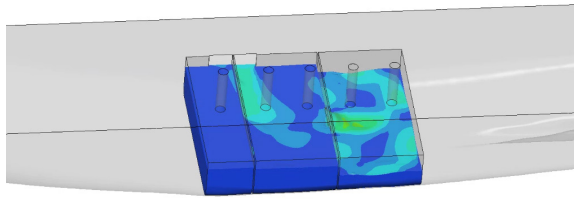

GM_2, t=6.6 s

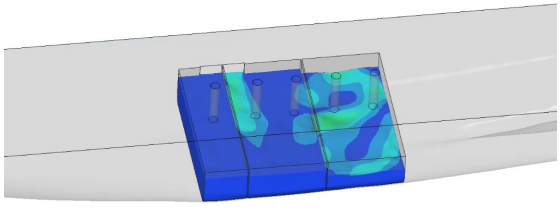

GM_1, t=7.0 s

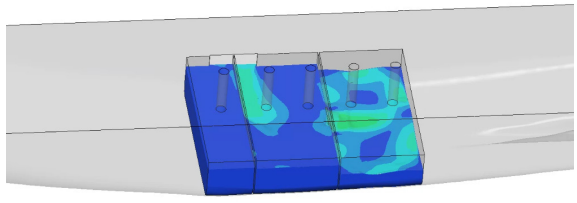

GM_2, t=7.0 s

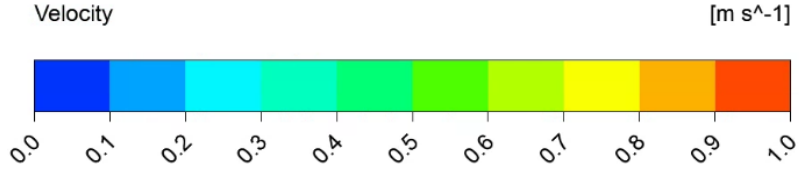

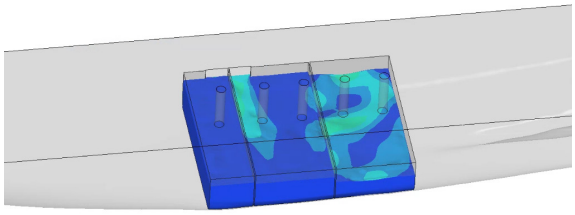

GM_1, t=7.4 s

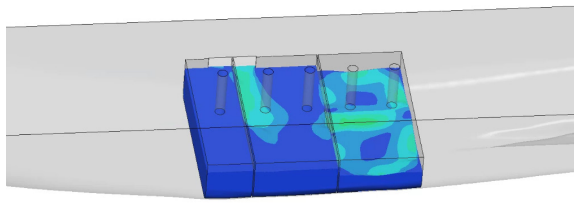

GM_2, t=7.4s

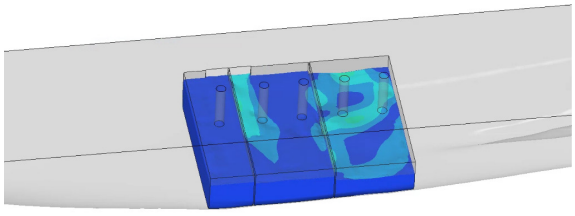

GM_1, t=7.8 s

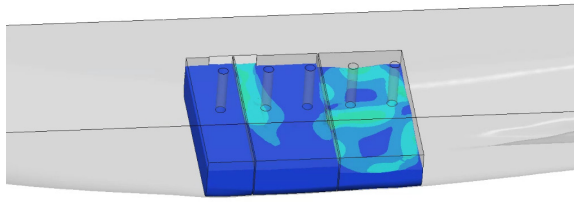

GM_2, t=7.8 s

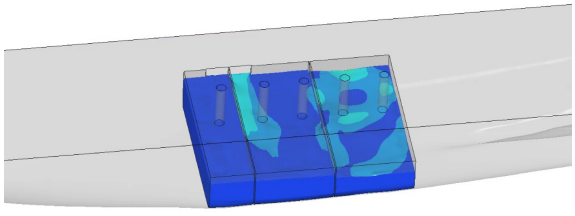

GM_1, t=8.2 s

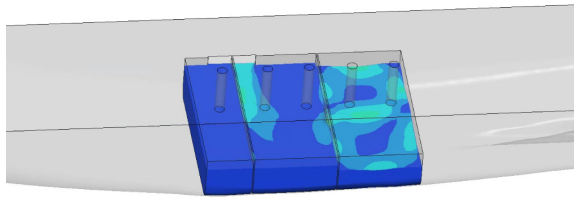

GM_2, t=8.2 s

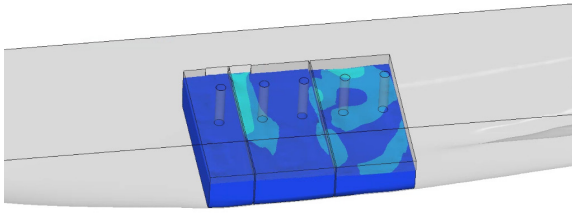

GM_1, t=8.6 s

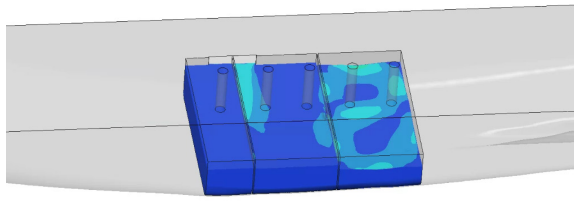

GM_2, t=8.6 s

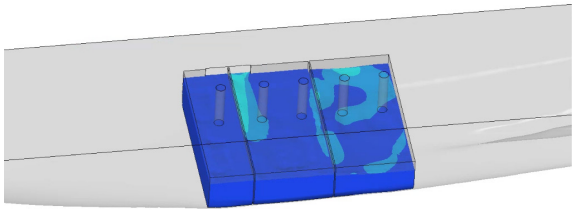

GM_1, t=9.0 s

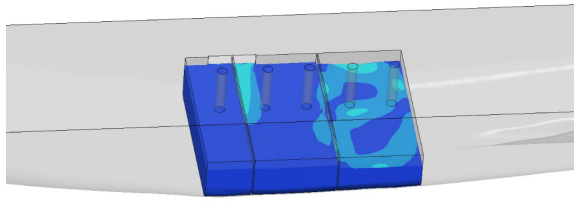

GM_2, t=9.0 s

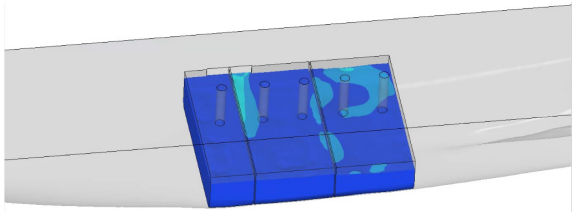

GM_1, t=9.4 s

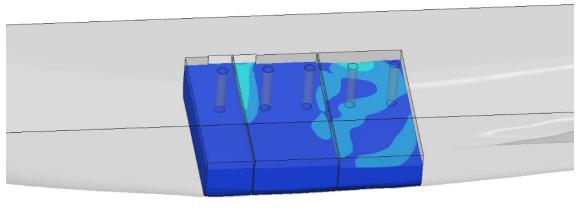

GM_2, t=9.4 s

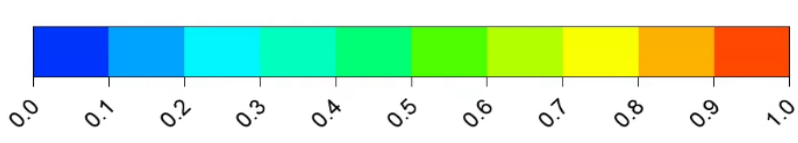

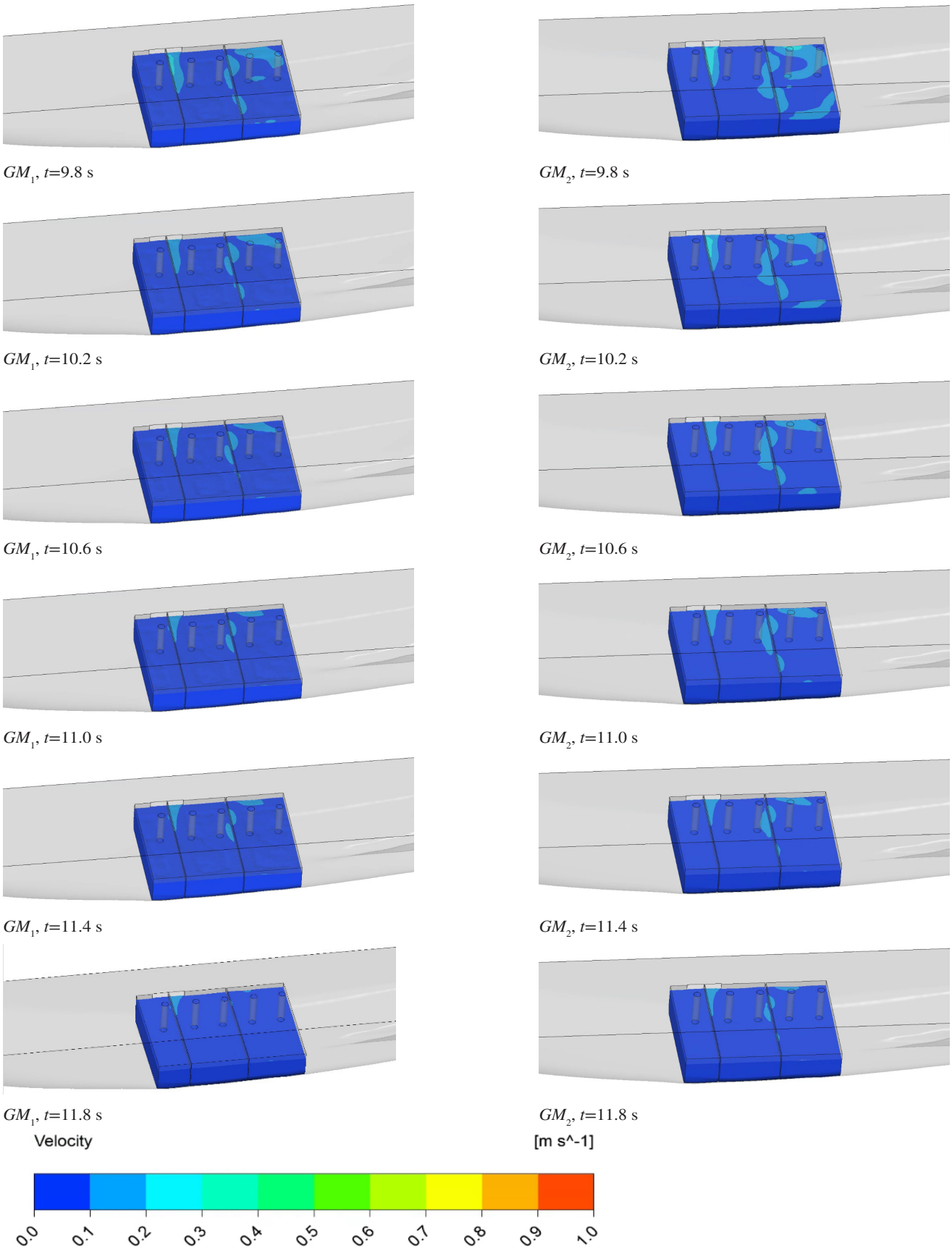

Figure 7. Visuals of the velocity colored flooding process for the initial stability conditions of GM_1 and GM_2

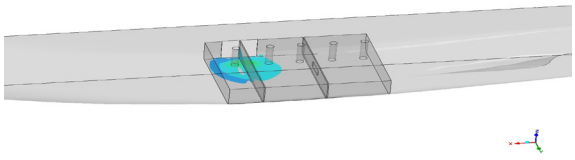

GM_1, t=0.2 s

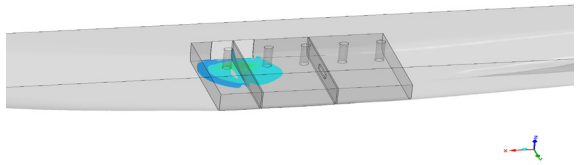

GM_2, t=0.2 s

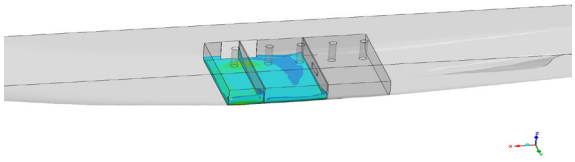

GM_1, t=0.6 s

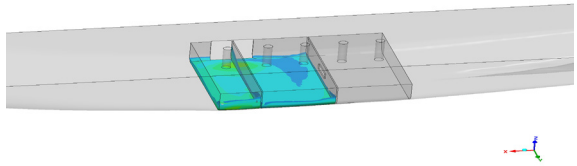

GM_2, t=0.6 s

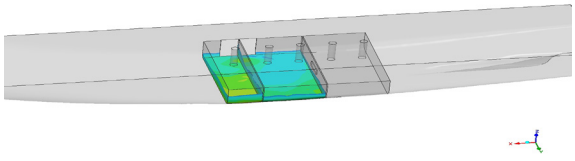

GM_1, t=1.0 s

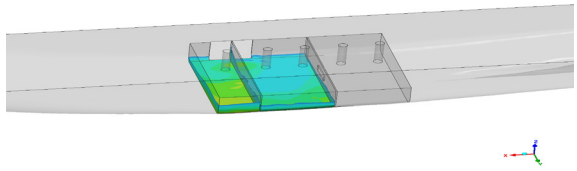

GM_2, t=1.0 s

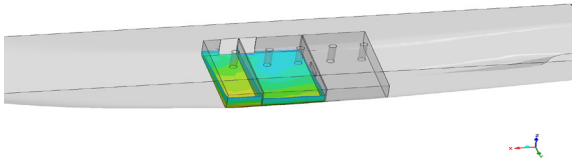

GM_1, t=1.4 s

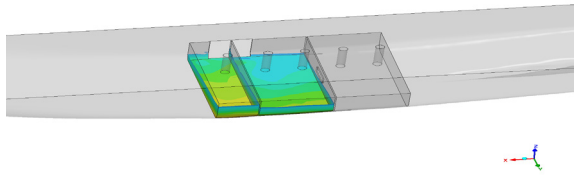

GM_2, t=1.4 s

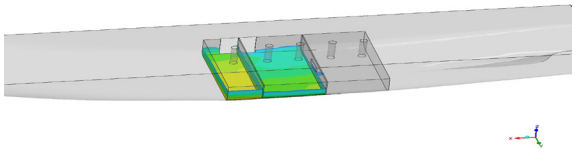

GM_1, t=1.8 s

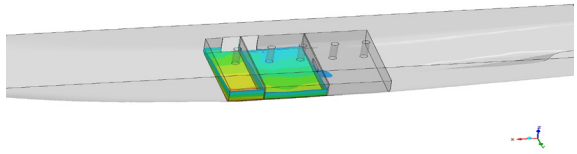

GM_2, t=1.8 s

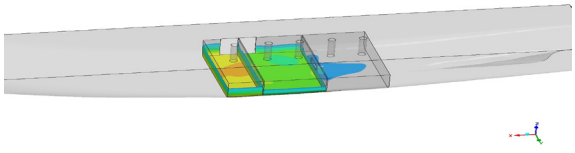

GM_1, t=2.2 s

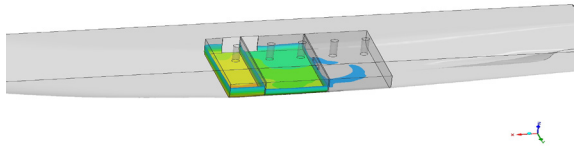

GM_2, t=2.2 s

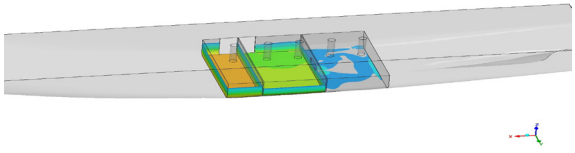

GM_1, t=2.6 s

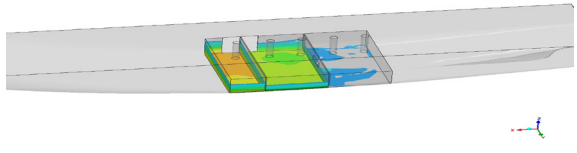

GM_2, t=2.6 s

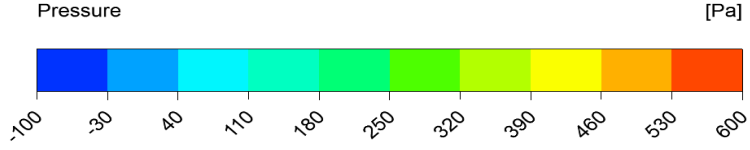

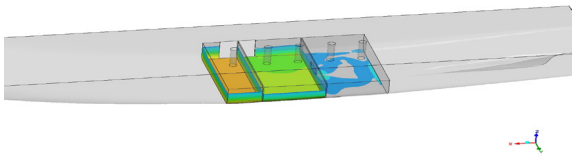

GM_1, t=2.6 s

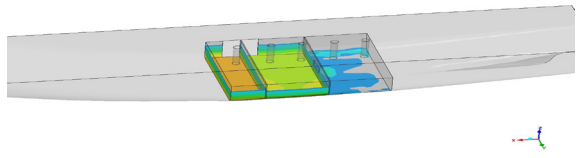

GM_2, t=2.6 s

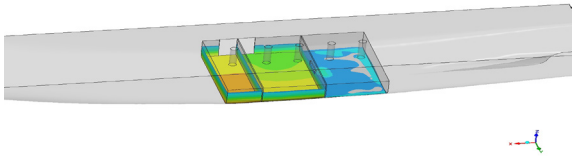

GM_1, t=3.0 s

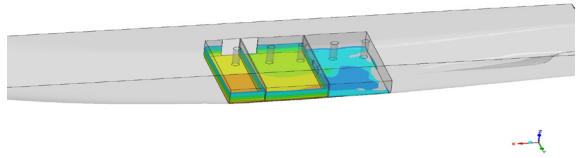

GM_2, t=3.0 s

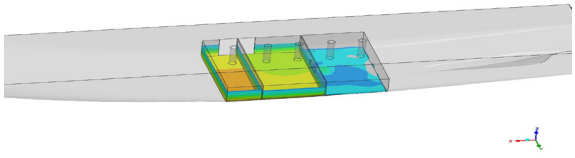

GM_1, t=3.4 s

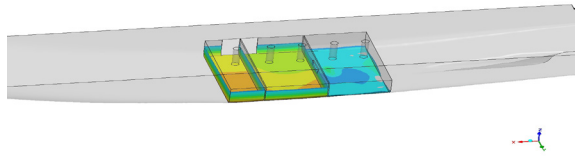

GM_2, t=3.4 s

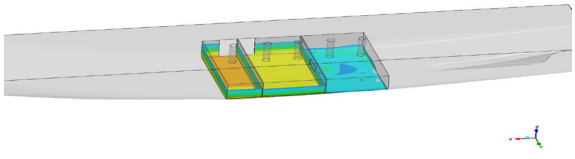

GM_1, t=3.8 s

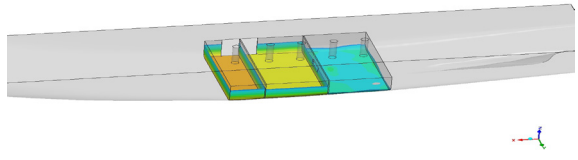

GM_2, t=3.8 s

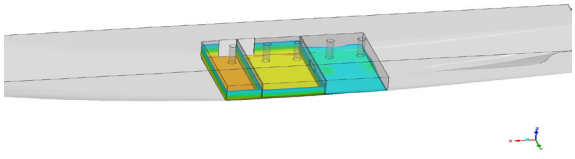

GM_1, t=4.2 s

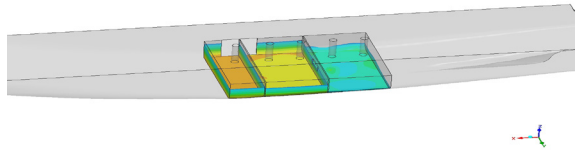

GM_2, t=4.2 s

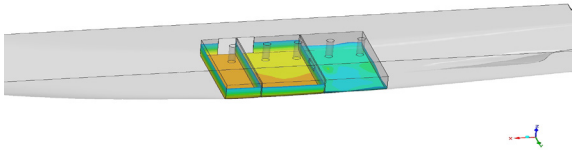

GM_1, t=4.6 s

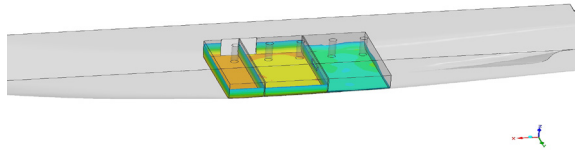

GM_2, t=4.6 s

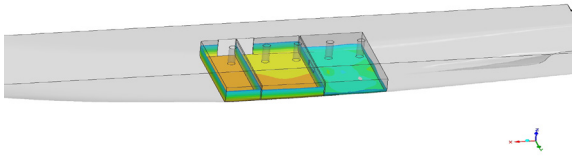

GM_1, t=5.0 s

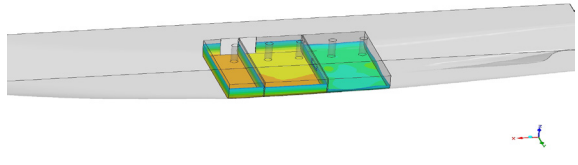

GM_2, t=5.0s

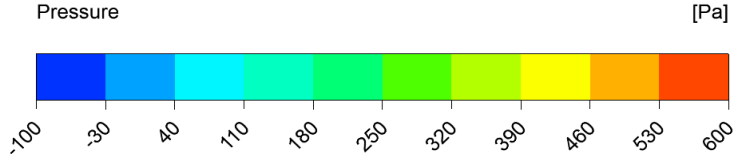

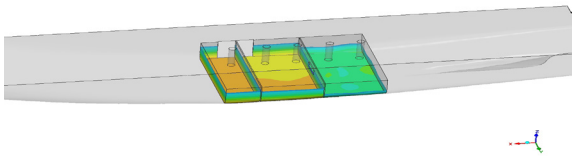

GM_1, t=5.4 s

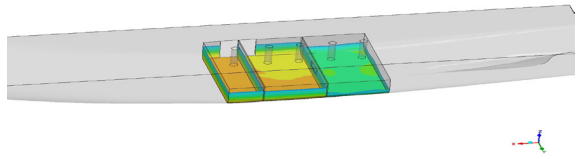

GM_2, t=5.4 s

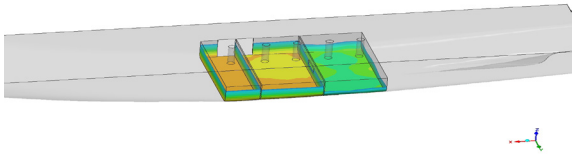

GM_1, t=5.8 s

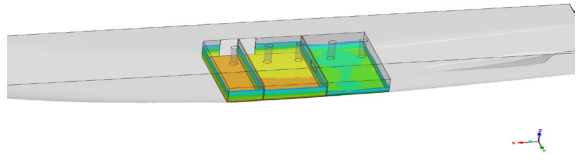

GM_2, t=5.8 s

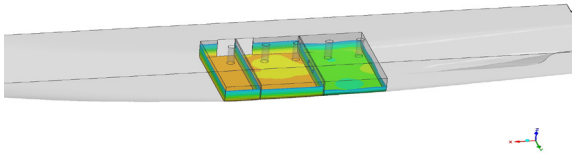

GM_1, t=6.2 s

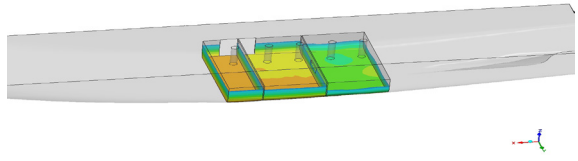

GM_2, t=6.2 s

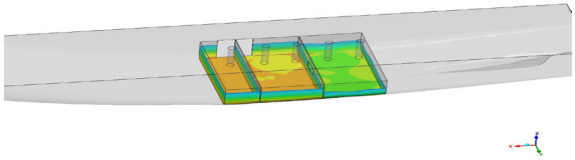

GM_1, t=6.6 s

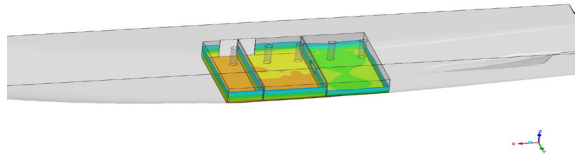

GM_2, t=6.6 s

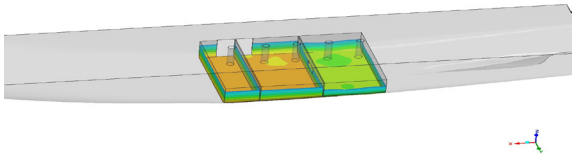

GM_1, t=7.0 s

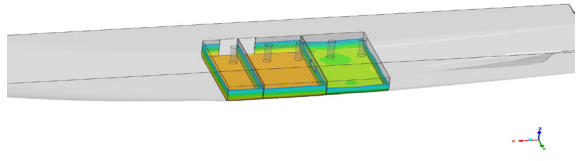

GM_2, t=7.0 s

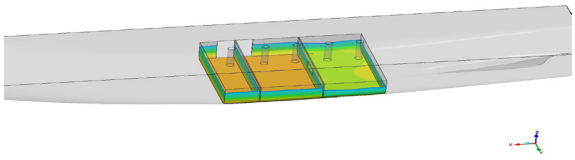

GM_1, t=7.4 s

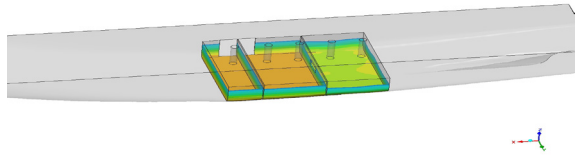

GM_2, t=7.4s

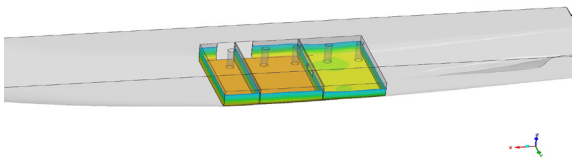

GM_1, t=7.8 s

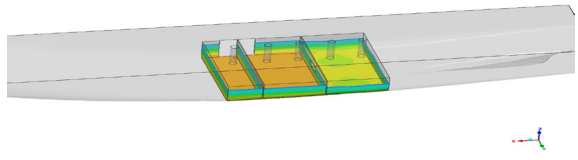

GM_2, t=7.8 s

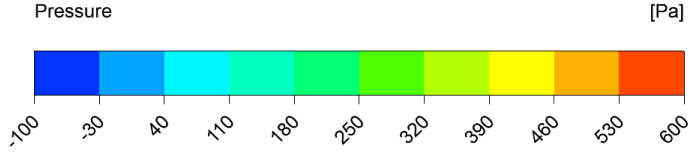

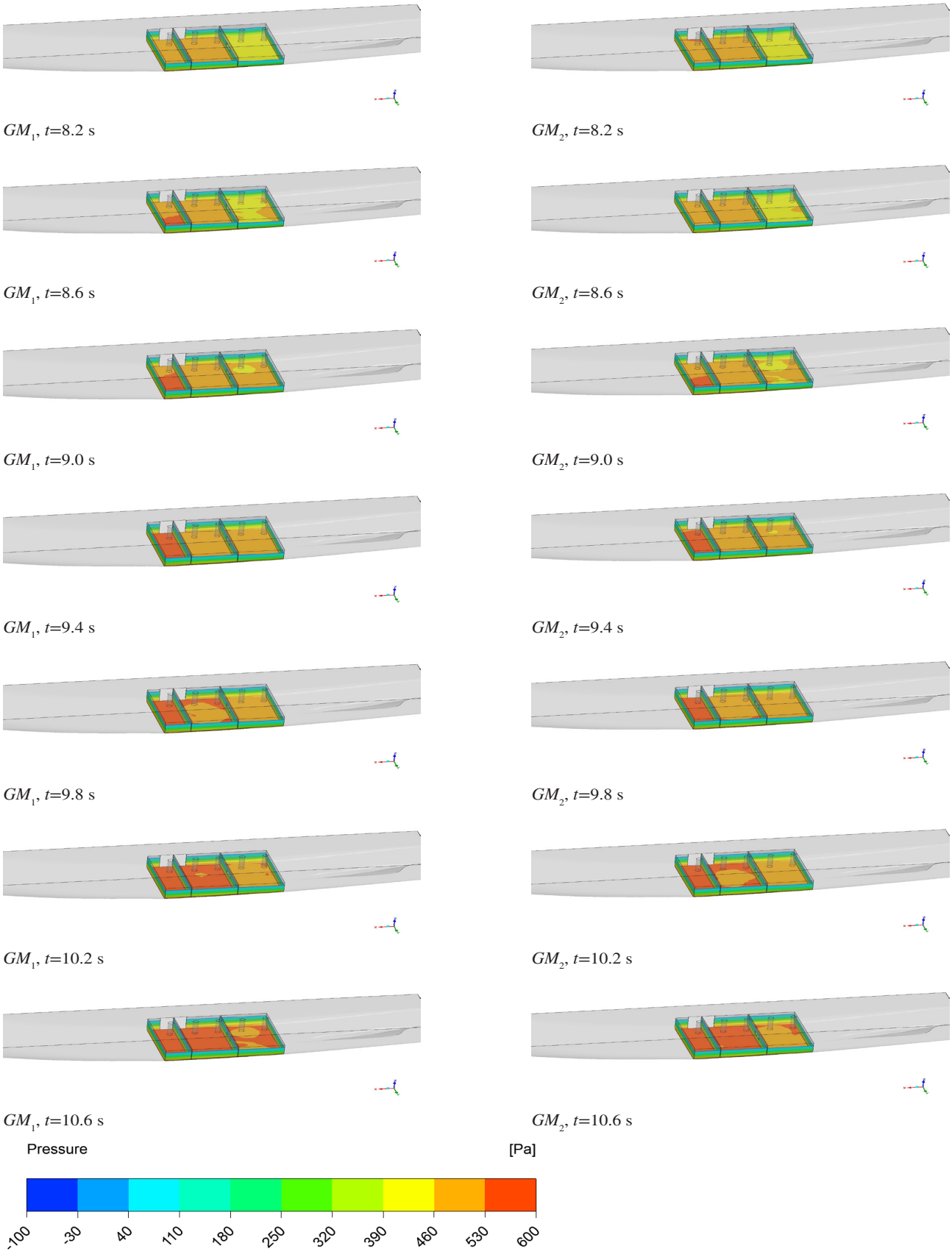

Figure 8. Visuals of pressure distributions on the walls of the damaged compartments caused by floodwater, under the initial stability conditions GM_1 and GM_2

4. Conclusion

This study investigated the influence of initial *GM* on the flooding behavior and motion response of a damaged Ro-Pax ship using RANS-based CFD analysis. The results show that differences in initial *GM* (GM_1 and GM_2) have a limited effect on the rate of water ingress. Both configurations reached similar floodwater masses, stabilizing at approximately 3.6 kg after 10 seconds, indicating that the flooding dynamics remained largely unaffected by *GM* variations within the observed period. In contrast, *GM* had a more pronounced impact on the vessel's motion response. Although both GM_1 and GM_2 configurations exhibited effective roll damping and ultimately converged to minimal roll angles, GM_1 showed reduced maximum roll amplitudes during the early stages of flooding. This behavior is associated with improved resistance to roll excitations induced by internal fluid motion, which is relevant for maintaining cargo security and dynamic stability. The effects of *GM* on pitch and heave motions were negligible, whereas yaw motion was more pronounced and less damped under lower stability conditions (GM_2). These findings highlight the relevance of selecting an appropriate *GM* in the damaged condition. Increasing *GM* can reduce roll and yaw motions during flooding, thereby lowering the risk of cargo displacement and subsequent instability. However, *GM* selection should also account for operational and comfort considerations, as excessive stability may lead to undesirable motion characteristics under normal operating conditions. Balancing these factors is essential to maintain both intact and damaged stability performance for Ro-Pax vessels.

Footnotes

Authorship Contributions

Concept: M. Z. Şener, H. K. Yoon, E. Köse, T. T. D. Nguyen, and A. CHO, Design: M. Z. Şener, H. K. Yoon, E. Köse, T. T. D. Nguyen, and A. CHO, Data Collection or Processing: M. Z. Şener, and T. T. D. Nguyen, Analysis or Interpretation: M. Z. Şener, and T. T. D. Nguyen, Literature Review: M. Z. Şener, H. K. Yoon, and E. Köse, Writing: M. Z. Şener, H. K. Yoon, E. Köse, T. T. D. Nguyen, and A. CHO.

Conflict of Interest: No conflict of interest was declared by the authors.

Financial Disclosure: The Scientific and Technological Research Council of Türkiye (TÜBİTAK) for the 2214-A International Doctoral Research Fellowship Programme for the first author, the Ship Dynamics and Control Laboratory of Changwon National University, and Karadeniz Technical University are all acknowledged for their support to make this work possible. This work was supported by the National Research Foundation of Korea (NRF) grant funded by the Korea government (MSIT) (NRF-2022R1A2C1093055).

5. References

[1] H. Cheng, A. M. Zhang, and F. R. Ming, "Study on coupled dynamics of ship and flooding water based on experimental and SPH methods," *Physics of Fluids,* vol. 29, no. 10, 107101, Oct 2017.

[2] X. Y. Cao, L. Tao, A.-M. Zhang, and F. R. Ming, "Smoothed particle hydrodynamics (SPH) model for coupled analysis of a damaged ship with internal sloshing in beam seas," *Physics of Fluids,* vol. 31, no. 3, 032103, Mar 2019.

[3] L.-F. Hu, H. Qi, Y. Li, W. Li, and S. Chen, "The CFD method-based research on damaged ship's flooding process in time-domain," *Polish Maritime Research,* vol. 26, no. 1, pp. 72-81, Mar 2019.

[4] J. Wang and D. Wan, "Application progress of computational fluid dynamic techniques for complex viscous flows in ship and ocean engineering," *Journal of Marine Science and Application,* vol. 19, pp. 1-16, Jun 2020.

[5] M. Xu, et al. "Advances in the application of intelligent algorithms to the optimization and control of hydrodynamic noise: Improve energy efficiency and system optimization," *Applied Sciences,* vol. 15, no. 4, pp. 2084, Feb 2025.

[6] Çakıcı, F., Kahramanoğlu E., Duman S., and Alkan, A. D. (2021) "Computational prediction of hydrodynamic coefficients for heave motion," *Seatific Journal*: Vol. 1: Iss. 1, Article 2.

[7] C. L. Navier, "Mémoire sur les lois du mouvement des fluides," *Mémoires de l'Académie Royale des Sciences de l'Institut de France,* pp. 389-440, 1823.

[8] G. G. Stokes, "On the theories of the internal friction of fluids in motion and of the equilibrium and motion of elastic solids," *Trans. Cambridge Philos. Soc.,* vol. 8, pp. 287-319, 1845.

[9] R. Osborne, "On the dynamical theory of incompressible viscous fluids and the determination of the criterion," *Philos. Trans. R. Soc. Lond.,* vol. 186, pp. 123-164, 1895.

[10] J. Boussinesq, "Essai sur la théorie des eaux courantes," *Mém. Présentés Divers Savants Acad. Sci.,* vol. 23, no. 1, pp. 1-680, 1877.

[11] A. Busemann, "Ludwig Prandtl, 1875-1953," *Biogr. Mem. Fellows R. Soc.,* vol. 5, pp. 193-205, Feb 1960.

[12] ANSYS, Inc., Ansys Fluent Theory Guide: Shear-Stress Transport (SST) k-ω Models. Canonsburg, PA: ANSYS, Inc., 2009.

[13] P. Ruponen, et al. "Results of an international benchmark study on numerical simulation of flooding and motions of a damaged ropax ship," *Applied Ocean Research*, vol. 123, 103153, Jun 2022.

[14] Meyer Turku Shipyard, "Meyer Turku Shipyard," Accessed: Jul 17, 2025. [Online]. Available: https://www.meyerturku.fi/en/index.jsp

[15] International Maritime Organization, SOLAS: Consolidated Edition, 2020. London, U.K.: International Maritime Organization, 2020.

[16] ITTC, Model Tests on Damage Stability in Waves, 7.5-02-07-04.2, ITTC Quality System Manual, Recommended Procedures and Guidelines, 2017.